

1 **Supplementary materials**

2
3
4 **Continental-scale contributions to the global CFC-11 emission**
5 **increase between 2012 and 2017**

6
7
8 Lei Hu^{1,2}, Stephen A. Montzka², Fred Moore^{1,2}, Eric Hintsala^{1,2}, Geoff Dutton^{1,2}, M. Carolina Siso^{1,2},
9 Kirk Thoning², Robert W. Portmann³, Kathryn McKain^{1,2}, Colm Sweeney², Isaac Vimont^{1,2}, David
10 Nance^{1,2}, Bradley Hall², Steven Wofsy⁴

11
12 ¹ Cooperative Institute for Research in Environmental Sciences, University of Colorado-Boulder,
13 Boulder, CO, USA

14 ² Global Monitoring Laboratory, NOAA, Boulder, CO, USA

15 ³ Chemical Science Laboratory, NOAA, Boulder, CO, USA

16 ⁴ Department of Earth and Planetary Sciences, Harvard University, Boston, MA, USA

17
18 *Correspondence to:* Lei Hu (lei.hu@noaa.gov)

46 **Table S1.** A list of the 23 inversion ensembles considered for this study.

Inversion ID	Inversion configurations		
	Observations	Background	Prior emissions
1	Only flask measurements	Background 1 ^a	Population-density-based priors with global emissions of 67 Gg yr ⁻¹ for the HIPPO and ATom periods
2	Only flask measurements	Background 1	Population-density-based priors with global emissions of 40 Gg yr ⁻¹ for the HIPPO and ATom periods
3	Flask + in situ measurements	Background 1	Population-density-based priors with global emissions of 67 Gg yr ⁻¹ for the HIPPO and ATom periods
4	Flask + in situ measurements	Background 1	Population-density-based priors with global emissions of 40 Gg yr ⁻¹ for the HIPPO and ATom periods
5	Flask + in situ measurements	Background 2 ^b	Population-density-based priors with global emissions of 67 Gg yr ⁻¹ for the HIPPO and ATom periods
6	Flask + in situ measurements	Background 2	Population-density-based priors with global emissions of 67 Gg yr ⁻¹ for the HIPPO period and 87 Gg yr ⁻¹ for the ATom periods. The 20 Gg yr ⁻¹ increase was imposed over North America.
7	Flask + in situ measurements	Background 2	Population-density-based priors with global emissions of 67 Gg yr ⁻¹ for the HIPPO period and 87 Gg yr ⁻¹ for the ATom periods. The 20 Gg yr ⁻¹ increase was imposed over South America.
8	Flask + in situ measurements	Background 2	Population-density-based priors with global emissions of 67 Gg yr ⁻¹ for the HIPPO period and 87 Gg yr ⁻¹ for the ATom periods. The 20 Gg yr ⁻¹ increase was imposed over Africa
9	Flask + in situ measurements	Background 2	Population-density-based priors with global emissions of 67 Gg yr ⁻¹ for the HIPPO period and 87 Gg yr ⁻¹ for the ATom periods. The 20 Gg yr ⁻¹ increase was imposed over Europe.
10	Flask + in situ measurements	Background 2	Population-density-based priors with global emissions of 67 Gg yr ⁻¹ for the HIPPO period and 87 Gg yr ⁻¹ for the ATom periods. The 20 Gg yr ⁻¹ increase was imposed over Australia.
11	Flask + in situ measurements	Background 2	Population-density-based priors with global emissions of 67 Gg yr ⁻¹ for the HIPPO period and 87 Gg yr ⁻¹ for the ATom periods. The 20 Gg yr ⁻¹ increase was imposed over boreal Asia.
12	Flask + in situ measurements	Background 2	Population-density-based priors with global emissions of 67 Gg yr ⁻¹ for the HIPPO period and 87 Gg yr ⁻¹ for the ATom periods. The 20 Gg yr ⁻¹ increase was imposed over temperate eastern Asia.
13	Flask + in situ measurements	Background 2	Population-density-based priors with global emissions of 67 Gg yr ⁻¹ for the HIPPO period and 87 Gg yr ⁻¹ for the ATom periods. The 20 Gg yr ⁻¹ increase was imposed over temperate western Asia.

14	Flask + in situ measurements	Background 2	Population-density-based priors with global emissions of 67 Gg yr ⁻¹ for the HIPPO period and 87 Gg yr ⁻¹ for the ATom periods. The 20 Gg yr ⁻¹ increase was imposed over tropical Asia.
15	Flask + in situ measurements	Background 2	Population-density-based priors with global emissions of 87 Gg yr ⁻¹ for the HIPPO period and 67 Gg yr ⁻¹ for the ATom periods. The 20 Gg yr ⁻¹ decrease was imposed over North America.
16	Flask + in situ measurements	Background 2	Population-density-based priors with global emissions of 87 Gg yr ⁻¹ for the HIPPO period and 67 Gg yr ⁻¹ for the ATom periods. The 20 Gg yr ⁻¹ decrease was imposed over South America.
17	Flask + in situ measurements	Background 2	Population-density-based priors with global emissions of 87 Gg yr ⁻¹ for the HIPPO period and 67 Gg yr ⁻¹ for the ATom periods. The 20 Gg yr ⁻¹ decrease was imposed over Africa.
18	Flask + in situ measurements	Background 2	Population-density-based priors with global emissions of 87 Gg yr ⁻¹ for the HIPPO period and 67 Gg yr ⁻¹ for the ATom periods. The 20 Gg yr ⁻¹ decrease was imposed over Europe.
19	Flask + in situ measurements	Background 2	Population-density-based priors with global emissions of 87 Gg yr ⁻¹ for the HIPPO period and 67 Gg yr ⁻¹ for the ATom periods. The 20 Gg yr ⁻¹ decrease was imposed over Australia
20	Flask + in situ measurements	Background 2	Population-density-based priors with global emissions of 87 Gg yr ⁻¹ for the HIPPO period and 67 Gg yr ⁻¹ for the ATom periods. The 20 Gg yr ⁻¹ decrease was imposed over boreal Asia.
21	Flask + in situ measurements	Background 2	Population-density-based priors with global emissions of 87 Gg yr ⁻¹ for the HIPPO period and 67 Gg yr ⁻¹ for the ATom periods. The 20 Gg yr ⁻¹ decrease was imposed over temperate eastern Asia.
22	Flask + in situ measurements	Background 2	Population-density-based priors with global emissions of 87 Gg yr ⁻¹ for the HIPPO period and 67 Gg yr ⁻¹ for the ATom periods. The 20 Gg yr ⁻¹ decrease was imposed over temperate western Asia.
23	Flask + in situ measurements	Background 2	Population-density-based priors with global emissions of 87 Gg yr ⁻¹ for the HIPPO period and 67 Gg yr ⁻¹ for the ATom periods. The 20 Gg yr ⁻¹ decrease was imposed over tropical Asia.

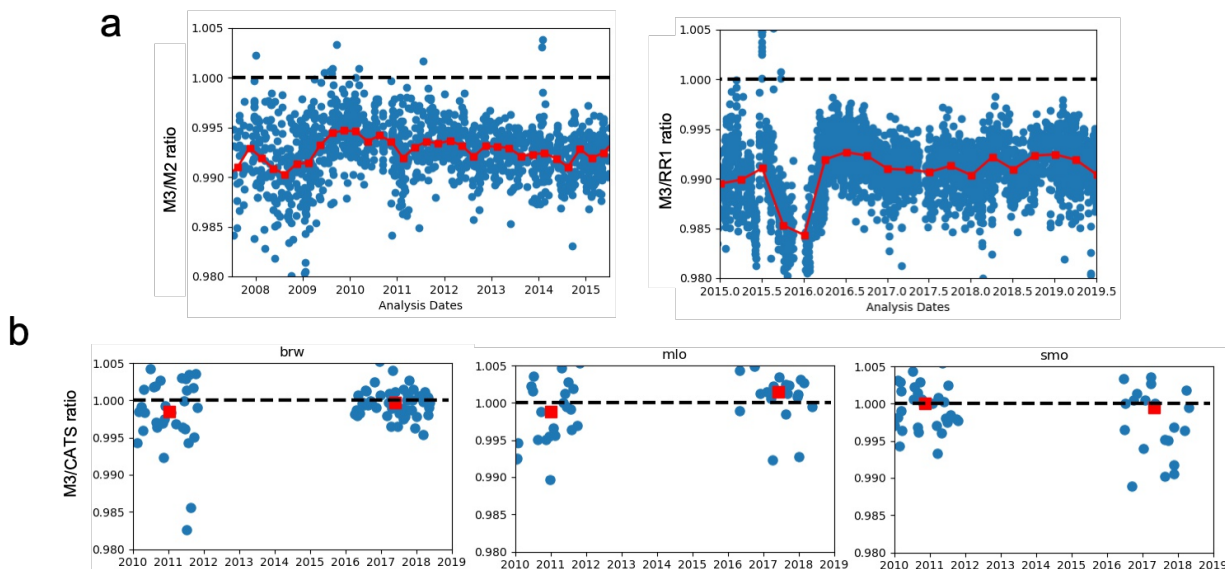
47 Notes:

48 a. With this background, the inversion-derived global emissions would be consistent with those estimated
49 from a 3-box model and an atmospheric lifetime of 52 years

50 b. With this background, the inversion-derived global emissions were consistent with those estimated from
51 a 3-box model and a lifetime of 54 - 56 years

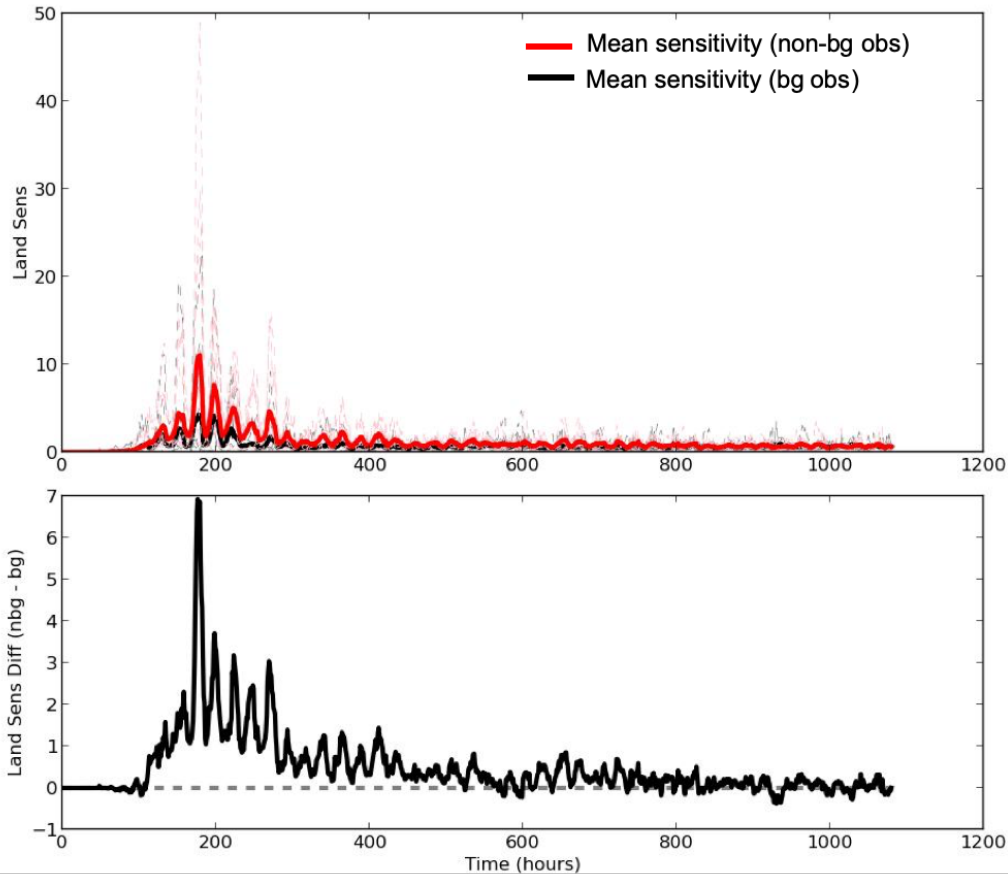
52

53



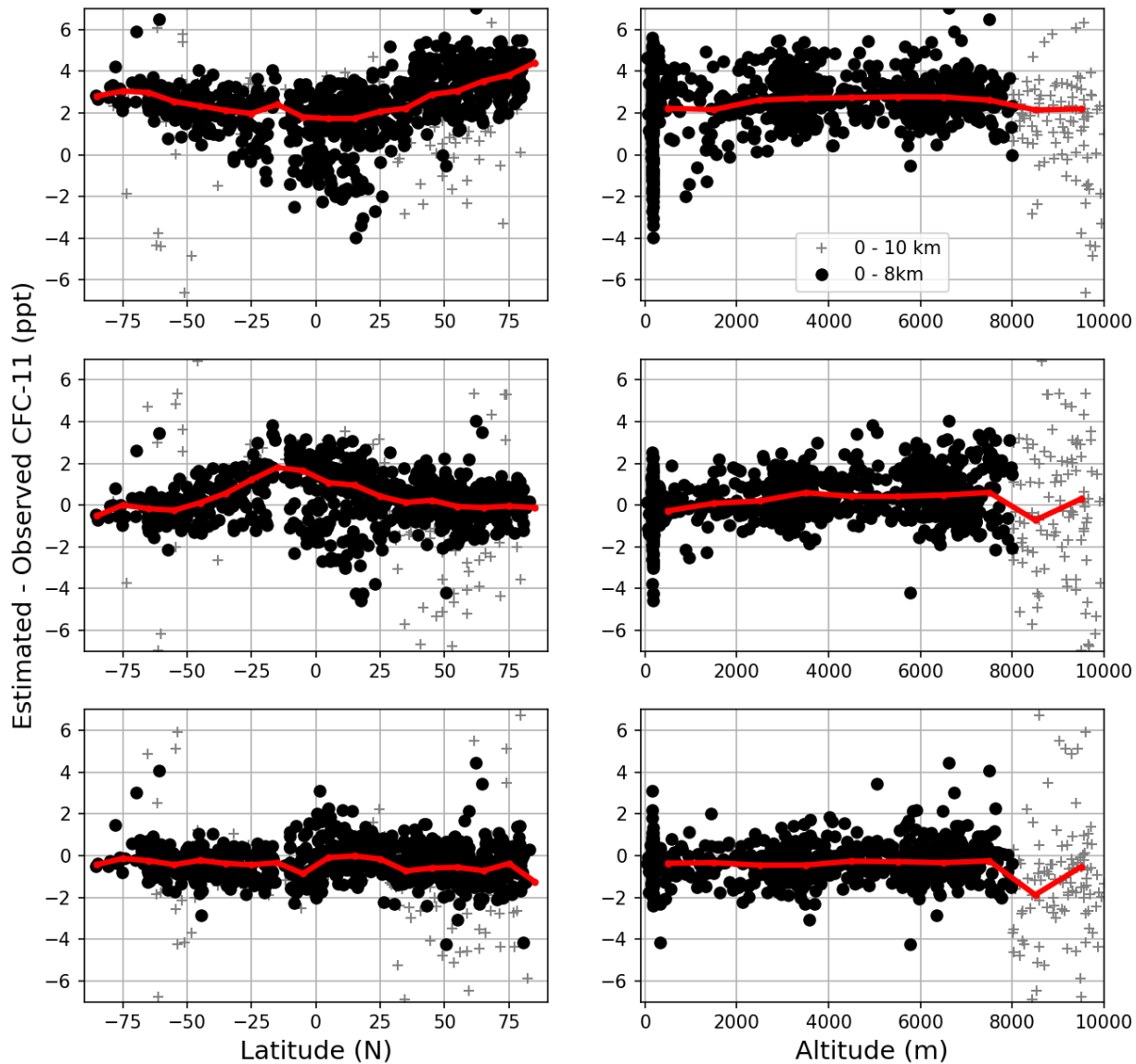
54
 55 **Fig. S1.** (a) Comparison of CFC-11 mole fractions ratios measured by three gas chromatograph
 56 and mass spectrometry (GCMS) instruments, named “M3”, “M2”, and “PR1” for the same flask-
 57 air samples. Blue symbols denote the measured raw mole fraction ratios between M3 and M2
 58 (left) and between M3 and PR1 (right). Red symbols indicate their three-month median ratios,
 59 which were used to improve consistency between measurements on these different instruments
 60 (see main text). (b) CFC-11 mole fraction ratios between flask-air samples analyzed by the M3
 61 GCMS instrument and in situ sampling that was collected within ± 2 hours of the flask-air samples
 62 and analyzed by in situ Electron Capture Detection instruments at three surface sites: Barrow,
 63 Alaska, United States (BRW), Mauna Loa, Hawaii, United States (MLO), and Tutuila, American
 64 Samoa (SMO). Red squares indicate the median scaling factors for the HIPPO and ATom periods,
 65 which were used to improve the measurement consistency (see main text).

66
 67
 68
 69
 70
 71
 72
 73
 74

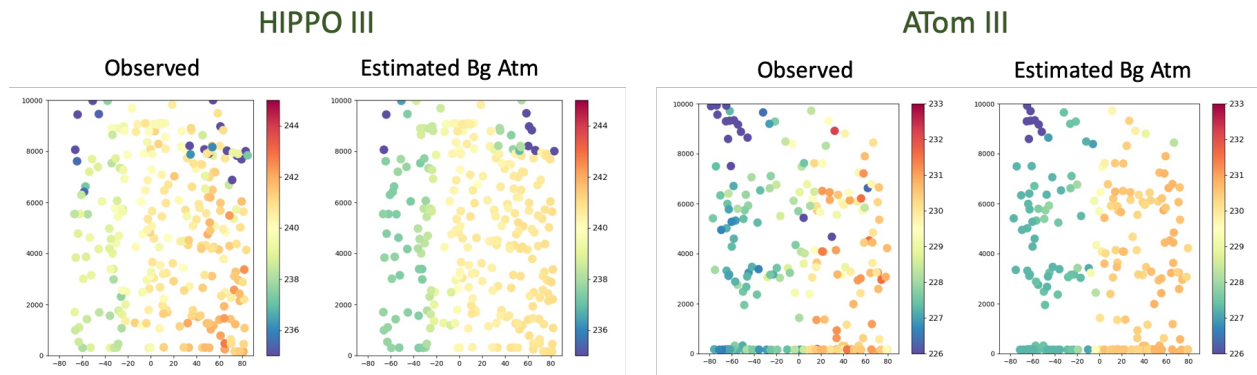


75
 76 **Fig. S2.** The upper panel shows the hourly footprint sensitivity in ppt ($\text{pmol m}^{-2} \text{s}^{-1}$)⁻¹ summed
 77 from land grid cells with above zero population for observations with mole fractions below the
 78 50%th percentile (black) and above the 50%th percentile (red), collected from the 30 – 60°N at
 79 500 – 750 hpa over the Pacific Ocean Basin from ATom II. Thin dashed lines represent the
 80 summed footprint for individual measurements, whereas the solid lines indicate the mean summed
 81 footprints from background and non-background observations. The lower panel indicates the
 82 difference between the red and black solid lines shown in the upper panel.

83
 84
 85
 86
 87
 88
 89

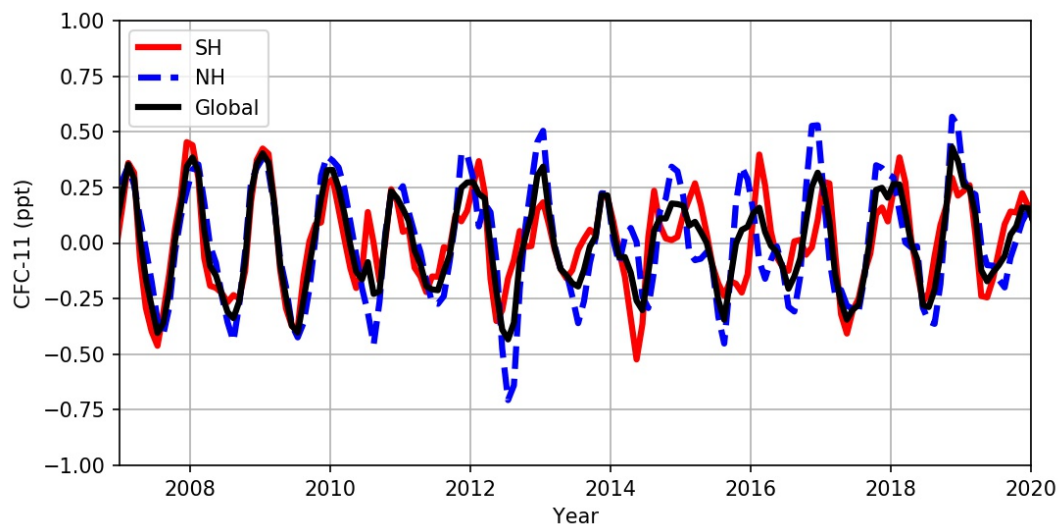


90
 91 **Fig. S3.** Residuals of the estimated and observed CFC-11 mole fractions for ATom I – IV
 92 campaigns, as a function of latitude (left panels) or altitude (right panels). (Upper panels)
 93 Estimated CFC-11 mole fractions were derived using the 4D mole fraction field from the WACCM
 94 simulation (see text). (Middle panels) Estimated CFC-11 mole fractions were derived using the
 95 WACCM 4D mole fraction field that was scaled to match the surface CFC-11 mole fractions
 96 observed in the NOAA’s global surface flask sampling network. (Lower panels) Estimated CFC-
 97 11 mole fractions were derived using a constructed 4D empirical background field. Back symbols
 98 indicate measurements made below 8 km, whereas black crosses indicate measurements above 8
 99 km. Red solid lines indicate mean biases calculated for bins of 10 degrees in latitudes (left panels)
 100 or 1 km of altitude (right panels).
 101



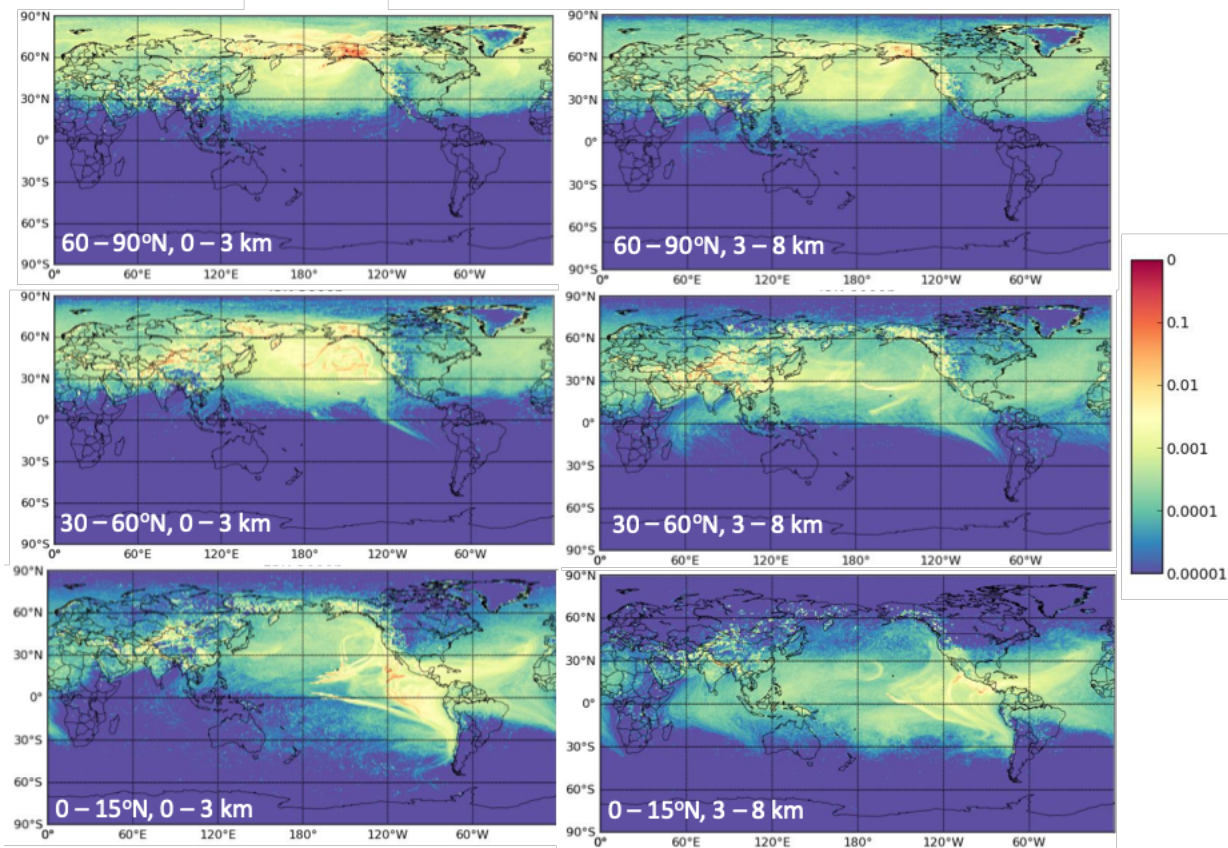
102
103
104
105
106
107
108

Fig. S4. Comparison of observed CFC-11 mole fractions and estimated background CFC-11 mole fractions (in ppt) for HIPPO III and ATom III campaigns using the 4D empirical background field.



109
110
111
112
113
114
115
116
117
118

Fig. S5. The seasonal cycle of global and hemispheric mean CFC-11 mole fractions. Data for this calculation is from <ftp://aftp.cmdl.noaa.gov/hats/cfcs/cfc11/combined/>. The seasonal cycle was calculated based on the global and hemispheric mean CFC-11 mole fractions subtracted by their 12 month running means.



119
 120 **Fig. S6.** Average sensitivity of ATom I and II flask-air samples collected between 0 and 8 km to
 121 upwind emissions. The observations were divided into 6 categories average 30° in latitudes and
 122 between 0 – 3 km and 3 – 8 km.
 123
 124